Finite Element Analysis of Linear Boundary Value Problems with Geometrical Parameters

R. Dyczij-Edlinger and O. Farle
Theoretische Elektrotechnik, Universität des Saarlandes, Campus, D-66123 Saarbrücken, Germany
E-mail: edlinger@lte.uni-saarland.de

***Abstract*: Traditional finite element analysis requires all system data, such as operating frequency, material properties, or geometrical specifications, to be given. In this paper, we propose a methodology that treats such quantities as variables. The resulting reduced-order models are of comparable accuracy but much smaller size than the original finite element systems and preserve important system properties such as reciprocity. We first review the theory for polynomial parameter-dependence and then analyze in detail a class of non-polynomial models arising from geometrical parameters.**

***Keywords*: Finite element method, model-order reduction.**

I. Introduction

The finite element (FE) method is a powerful numerical technique for the analysis of electromagnetic field problems and, thanks to the rapid development in computer hardware and software technology, runtimes for single solutions are oftentimes just in the order of minutes. However, when the system response is sought over a broad frequency range, or when multiple design parameters are present, such as in response surface modelling, shape optimization, or inverse problems, the number of FE evaluations becomes exceedingly large. In such cases, computer runtime is still a limiting factor.

For such purposes, methods of model-order reduction (MOR) are very effective, because the reduced-order models (ROMs) they produce are of low dimension and hence very cheap to analyze. Typical rates are in the order of some 10 to 100 function evaluations per second, using MATLAB on an ordinary PC. In the FE context, single-point methods are particularly attractive, because they require to factorize the underlying FE system at one expansion point only. Single-point algorithms for multiple parameters were presented in [1] – [6] . However, they were either restricted to multi-linear parameter-dependence [5] [6] or to small parameter domains [1] – [4] , due to numerical issues.

In a recent publication [7], we proposed a new approach that is not only numerically robust but also handles polynomial parameterization. The present work extends the scope of our method to FE systems featuring geometric parameters. In this case, the main difficulty is that the parameters enter the FE formulation in the form of multivariate rational functions. The rest of the paper is organized as follows: Section II summarizes the principles of multivariate MOR for polynomial parameter-dependence, which will be needed later on. Then, in Section III, we turn to non-polynomial models arising from geometric parameterization. The main contribution of this paper is Subsection III A, which presents the method, its limitations, and various sources of error. Numerical examples, including a study of different interpolation schemes, are given in Section IV.

II. Polynomial Parameter-Dependence

FE models with variable material data and/or working frequency exhibit polynomial parameter-dependence. Formally, we deal with a system of linear equations of dimension n, which is parameterized by a polynomial of order M in N scalar variables, $\mathbf{s} = (s_1, \ldots, s_N)$, and, in the single-input-single-output case, a scalar-valued transfer function $H(\mathbf{s})$. Using multi-index notation, we have

$$\Big(\sum_{|\alpha|<M} \mathbf{s}^\alpha \mathbf{A}_\alpha\Big)\mathbf{x} = \Big(\sum_{|\alpha|<M} \mathbf{s}^\alpha \mathbf{b}_\alpha\Big)u, \tag{1a}$$

$$y = \mathbf{c}^*\mathbf{x}, \tag{1b}$$

$$H(\mathbf{s}) = \mathbf{c}^*\Big(\sum_{|\alpha|<M} \mathbf{s}^\alpha \mathbf{A}_\alpha\Big)^{-1}\sum_{|\alpha|<M} \mathbf{s}^\alpha \mathbf{b}_\alpha. \tag{1c}$$

The MOR methods we consider [7] share a common structure: they are Bubnov-Galerkin methods and employ well-chosen pairs of matrices $\mathbf{V} \in \mathbb{C}^{n\times m}$ and $\mathbf{W} \in \mathbb{C}^{n\times m}$ to restrict the trial and test spaces of the original FE matrices. Hence the resulting reduced-order vectors and matrices take the form

$$\hat{\mathbf{x}}(\mathbf{s}) = \mathbf{V}\mathbf{z}(\mathbf{s}), \tag{2a}$$

$$\hat{\mathbf{b}}_\alpha = \mathbf{W}^*\mathbf{b}_\alpha, \tag{2b}$$

$$\hat{\mathbf{A}}_\alpha = \mathbf{W}^*\mathbf{A}_\alpha\mathbf{V}, \tag{2c}$$

$$\hat{\mathbf{c}}^* = \mathbf{c}^*\mathbf{V}, \tag{2d}$$

and the reduced-order transfer function $\hat{H}(\mathbf{s})$ reads

$$\hat{H}(\mathbf{s}) = \hat{\mathbf{c}}^*\Big(\sum_{|\alpha|<M} \mathbf{s}^\alpha \hat{\mathbf{A}}_\alpha\Big)^{-1}\sum_{|\alpha|<M} \mathbf{s}^\alpha \hat{\mathbf{b}}_\alpha. \tag{2e}$$

As long as the ROM is of much lower dimension than the original system, $m \ll n$, it can be evaluated very efficiently at any point $\mathbf{s}$ in parameter space. Obviously, the quality of the ROM is greatly influenced by the choice of trial and test spaces colsp$\mathbf{V}$ and colsp$\mathbf{W}$. Specific methods differ in the construction of $\mathbf{V}$ and $\mathbf{W}$, but are generally combinations of the following two prototypes: multi-point methods are based on the interpolation property

$$\hat{\mathbf{x}}(\mathbf{s}_p) = \mathbf{x}(\mathbf{s}_p) \qquad \text{for } p = 1 \ldots P, \tag{3}$$

whereas single-point methods consider one expansion point $\mathbf{s}_0$ only, at which all moments up to order Q of $\hat{H}$ are made to coincide with those of H,

$$\frac{\partial^{|q|}\hat{H}}{\partial \mathbf{s}^q}\Big|_{\mathbf{s}_0} = \frac{\partial^{|q|}H}{\partial \mathbf{s}^q}\Big|_{\mathbf{s}_0} \qquad \text{for } |q| < Q. \tag{4}$$

The advantage of single-point methods is that they just require one FE solution. Once a factorization of the FE matrix at the expansion point is available, a sequence of inexpensive forward-back substitutions suffices to generate the entire ROM. However, the design of robust single-point algorithms is more delicate than in the multi-point case.

A. Single-Point Algorithm

Since the formal treatment of single-point ROMs for systems that depend on arbitrary numbers of parameters and polynomials of arbitrary order is very technical, we restrict ourselves to the case of quadratic dependence on two parameters s_1 and s_2,

$$\begin{aligned}\left(\mathbf{A}_{00}+s_1\mathbf{A}_{10}+s_2\mathbf{A}_{01}+s_1^2\mathbf{A}_{20}+s_1s_2\mathbf{A}_{11}+s_2^2\mathbf{A}_{02}\right)\mathbf{x}\\ =\left(\mathbf{b}_{00}+\ldots+s_2^2\mathbf{b}_{02}\right)u,\end{aligned} \tag{5}$$

wherein $\mathbf{A}_{00}$ is required to be invertible. Without loss of generality, we set $u = 1$ and expand the solution vector $\mathbf{x}$ of (5) in a Taylor series,

$$\begin{aligned}\left(\mathbf{A}_{00}+s_1\mathbf{A}_{10}+\ldots+s_2^2\mathbf{A}_{02}\right)\left(\sum_{e=0}^{\infty}\sum_{i=0}^{e}s_1^i s_2^{e-i}\mathbf{x}_{i,e-i}\right)\\ =\mathbf{b}_{00}+s_1\mathbf{b}_{10}+\ldots+s_2^2\mathbf{b}_{02}.\end{aligned} \tag{6}$$

By comparison of coefficients, we have

$$\mathbf{x}_{00}=\mathbf{A}_{00}^{-1}\mathbf{b}_{00} \tag{7a}$$
$$\mathbf{x}_{10}=\mathbf{A}_{00}^{-1}\left(\mathbf{b}_{10}-\mathbf{A}_{10}\mathbf{x}_{00}\right) \tag{7b}$$
$$\vdots$$
$$\mathbf{x}_{30}=\mathbf{A}_{00}^{-1}\left(-\mathbf{A}_{10}\mathbf{x}_{20}-\mathbf{A}_{20}\mathbf{x}_{10}\right) \tag{7c}$$
$$\vdots$$
$$\begin{aligned}\mathbf{x}_{ij}=\mathbf{A}_{00}^{-1}(&-\mathbf{A}_{10}\mathbf{x}_{i-1,j}-\mathbf{A}_{01}\mathbf{x}_{i,j-1}-\mathbf{A}_{20}\mathbf{x}_{i-2,j}\\ &-\mathbf{A}_{11}\mathbf{x}_{i-1,j-1}-\mathbf{A}_{02}\mathbf{x}_{i,j-2}).\end{aligned} \tag{7d}$$

The recursion (7) defines a parameter-independent subspace spanned by all $\mathbf{x}_{ij}$ with $i + j \leq q$, the *multivariate Krylov space of order two*, $\mathcal{K}_q\left(\mathbf{A}_{00}^{-1}\mathbf{A}_{kl}, \mathbf{A}_{00}^{-1}\mathbf{b}_{kl}\right)$,

$$\mathcal{K}_q\left(\mathbf{A}_{00}^{-1}\mathbf{A}_{kl}, \mathbf{A}_{00}^{-1}\mathbf{b}_{kl}\right)=\operatorname{span}\{\mathbf{x}_{ij}\big|i+j\leq q\}. \tag{8}$$

Hence, when the trial matrix $\mathbf{V}$ is chosen such that

$$\operatorname{colsp}\mathbf{V}=\mathcal{K}_q\left(\mathbf{A}_{00}^{-1}\mathbf{A}_{kl}, \mathbf{A}_{00}^{-1}\mathbf{b}_{kl}\right), \tag{9}$$

the reduced transfer function $\hat{H}$ will possess the moment-matching property (4). A rigorous proof is by induction.

An analogous derivation shows that the number of matching moments increases to $2q + 1$, when $\mathbf{W}$ is constructed such that

$$\operatorname{colsp}\mathbf{W}=\mathcal{K}_q\left(\mathbf{A}_{00}^{*-1}\mathbf{A}_{kl}^{*}, \mathbf{A}_{00}^{*-1}\mathbf{c}_{kl}\right), \tag{10}$$

$$\mathbf{c}_{kl}=\begin{cases}\mathbf{c} & \text{for } (k,l)=(0,0),\\ \mathbf{0} & \text{else.}\end{cases} \tag{11}$$

A.1. Algorithmic Considerations

For improved numerical robustness, our actual algorithm does not implement the recursion (7) directly. Rather, we employ orthogonal bases for the Krylov spaces (8) and (10). See [7] for details.

B. Numerical Example

Fig. 1 presents the structure of a patch antenna from [8]. We analyze the behavior of the reflection coefficient S_{11} as a function of operating frequency f and the relative permittivities of the two substrate layers, ε_{r1} and ε_{r2}. For this purpose, we set the expansion point at ($\bar{f}$ = 6 GHz, $\bar{\varepsilon}_{r1}$ = 4, $\bar{\varepsilon}_{r2}$ = 2) and introduce the following parameterization:

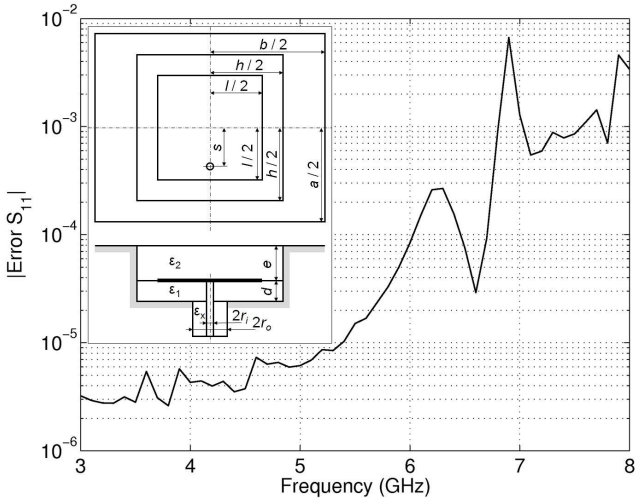

Figure 1. Error in S_{11} versus frequency for ε_{r1} = 1, ε_{r2} = 3. Inset shows structure of patch antenna with ε_x=1.951. Dimensions (in mm): a=22.15, b=47.45, h=18.15, l=13.5, s=1.75, d=2.42, e=2.6, r_i=0.64, r_0=2.05.

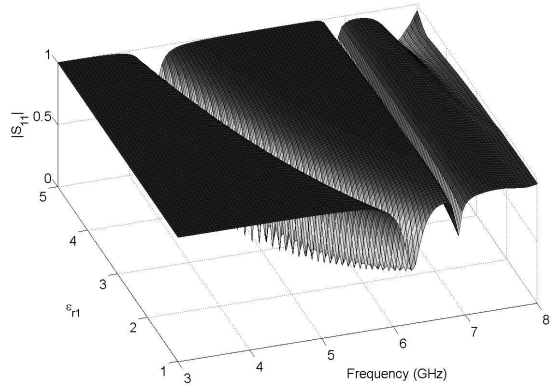

Figure 2. Magnitude of reflection coefficient $|S_{11}|$ at $\varepsilon_{r2} = 3$ as function of frequency and relative permittivity ε_{r1}.

$$\omega=\bar{\omega}(1+s_1), \tag{12a}$$
$$\varepsilon_1=\bar{\varepsilon}_1(1+s_2), \tag{12b}$$
$$\varepsilon_2=\bar{\varepsilon}_2(1+s_3). \tag{12c}$$

The resulting FE system is of the form

$$\begin{aligned}\{&-s_1s_2 2\bar{\omega}^2\mathbf{T}_1-s_1s_3 2\bar{\omega}^2\mathbf{T}_2-s_1^2s_2\bar{\omega}^2\mathbf{T}_1-s_1^2s_3\bar{\omega}^2\mathbf{T}_2\\ &-s_2\bar{\omega}^2\mathbf{T}_1-s_3\bar{\omega}^2\mathbf{T}_2-s_1^2\bar{\omega}^2\left(\mathbf{T}+\bar{\varepsilon}_1\mathbf{T}_1+\bar{\varepsilon}_2\mathbf{T}_2\right)\\ &-s_1[2\bar{\omega}^2\left(\mathbf{T}+\bar{\varepsilon}_1\mathbf{T}_1+\bar{\varepsilon}_2\mathbf{T}_2\right)-j\bar{\omega}\tilde{\mathbf{I}}-\bar{\omega}\mathbf{T}_R]\\ &+\mathbf{S}-\bar{\omega}^2\left(\mathbf{T}+\bar{\varepsilon}_1\mathbf{T}_1+\bar{\varepsilon}_2\mathbf{T}_2\right)+\bar{\omega}\mathbf{T}_R+j\bar{\omega}\tilde{\mathbf{I}}\}\mathbf{x}\\ &=\bar{\omega}\mathbf{b}+s_1\bar{\omega}\mathbf{b}\end{aligned} \tag{13}$$

and results in $n = 58247$ second order degrees of freedom, whereas the dimension of a reduced model of order $q = 8$ is just 165. As a result, we obtain 68.5 ROM evaluations per second, using interpreted MATLAB code. ROM generation takes 983.3 s. The comparison with full FE solutions in Fig. 1 shows that the accuracy of the ROM is very satisfactory. A two-dimensional cut through the response hyper-surface can be seen in Fig. 2.

III. Geometric Parameters

In contrast to the parameters considered in Section II, geometry enters the finite element (FE) method in discretized

form and results in dependencies that are multivariate rational functions of complicated nature.

To characterize the situation, we first consider a single finite element. Each of its nodes can be endowed with at most three geometry parameters, one for each spatial direction. While the element matrices are invariant under the six rigid body transformations, their dependence of the remaining degrees of freedom is given by rational functions. For instance, when the element size h is rescaled, the mass matrix $\mathbf{T}_{el}$ changes proportionally to h, whereas the variation of the stiffness matrix $\mathbf{S}_{el}$ is proportional to $1/h$. In case of general deformations, rational functions of even higher order emerge.

During the assembly process, various fractional terms are being summed up. As a result, the entries of the global FE matrices are given by multivariate rational functions of high order whose denominators may differ entry by entry.

In consequence, we face the following challenges and limitations:

- The discrete nature of geometry representation in the FE method poses a principal limitation on the applicability of the MOR methods considered: since parameter dependence must be smooth, topological changes in the mesh are not permissible. Hence all parameter variations must be small enough so that the corresponding FE meshes can be obtained from a single nominal discretization by continuous deformation. Otherwise one has to resort to meta-modelling techniques [9] [10], which in turn may utilize the proposed MOR approach as a fast subdomain solver.
- The MOR method of Section II requires polynomial parameter-dependence, whereas the FE matrices are of rational type. Since denominators are entry-specific and of high degree, multiplication by the smallest common multiple is not an option. Therefore, approximation methods are required to obtain systems of type (1c).
- Finally, the construction of parameter-dependent FE matrices and right-hand-side (RHS) vectors requires parametric information to propagate from the solid model through the meshing process to the core of the FE solver. Rigorous construction, especially in case of multiple parameters, requires tools like automatic differentiation or symbolic algebra, which may not be viable for complicated real-world problems.

A. Proposed Method

In view of the arguments above, we have to cope with the fact that explicit parameter dependence at the FE level may generally not be available. Therefore, we propose to take a more direct but approximate approach:

1) Mesh parameterization. Given a nominal mesh $\mathcal{M}_0$ at the expansion point, we construct a parametric mesh $\mathcal{M}(\mathbf{s})$ with the following properties:
   a) The node positions of $\mathcal{M}(\mathbf{s})$ are smooth functions of parameters $\mathbf{s}$.
   b) $\mathcal{M}(\mathbf{s})$ is topologically equivalent to $\mathcal{M}_0$.
   c) $\mathcal{M}(\mathbf{s})$ is a valid FE mesh over the entire parameter domain.
2) Interpolation. We interpolate the parameter dependence of the FE system by multivariate polynomials of low order $p_\beta(\mathbf{s})$ [11]. For this purpose, we instantiate the mesh at a unisolvent set of sampling points $\mathbf{s}_\beta$ in parameter space, at which we assemble the global FE matrix $\mathbf{A}(\mathbf{s}_\beta)$ and the RHS vector $\mathbf{b}(\mathbf{s}_\beta)$. The resulting interpolations $\tilde{\mathbf{A}}(\mathbf{s})$ and $\tilde{\mathbf{b}}(\mathbf{s})$ are given by

$$\tilde{\mathbf{A}}(\mathbf{s}) = \sum_\beta p_\beta(\mathbf{s})\mathbf{S}(\mathbf{s}_\beta), \tag{14a}$$

$$\tilde{\mathbf{b}}(\mathbf{s}) = \sum_\beta p_\beta(\mathbf{s})\mathbf{b}(\mathbf{s}_\beta) \tag{14b}$$

   and result in a parameterized system of type (1c), as required. In case that matrices or vectors of different physical nature, such as stiffness and mass matrices, are present, we interpolate each of them separately.
3) MOR for polynomial parameter-dependence. See Section II.

The major advantage of our strategy is that parameterization is kept away from low-level FE computations, and that multivariate rational functions are never handled explicitly. The obvious disadvantage is its approximate nature.

A.1. Types of Errors

Each stage of our method is associated with a specific kind of error. Specifically, we have:

- *Mesh deformation error:* Large changes in geometry lead to large mesh deformations, which in turn may result in poor mesh quality, as illustrated in Fig. 4. The latter may negatively affect the approximation properties of the FE model. In addition, the field distribution may change so much that the FE discretization becomes to coarse in some critical regions.
- *Interpolation error:* In between sampling points, the interpolated system

$$\tilde{\mathbf{A}}(\mathbf{s})\tilde{\mathbf{x}}(\mathbf{s}) = \tilde{\mathbf{b}}(\mathbf{s}) \tag{15}$$

  does not coincide with the original one,

$$\mathbf{A}(\mathbf{s})\mathbf{x}(\mathbf{s}) = \mathbf{b}(\mathbf{s}). \tag{16}$$

  Therefore, the resulting transfer functions, $\tilde{H}(\mathbf{s})$ and $H(\mathbf{s})$, differ. The quality of (15) depends not only on the degree of the interpolation polynomial but also the choice of sampling points.
- *MOR error:* This is the error committed by approximating the interpolated system (15) by the ROM (2).

IV. Numerical Examples

The main purpose of our first example, a simple waveguide iris, is to compare different interpolation schemes and to quantify the errors associated with each stage of approximation. The second example demonstrates the applicability of the proposed method to real-world filter configurations.

A. Metal Iris

We consider a metal iris of zero thickness within a rectangular waveguide with $\mu_r = \varepsilon_r = 1$. As indicated by Fig. 3, just one quarter of the structure has been modelled. We compute the reflection coefficient S_{11} as a function of

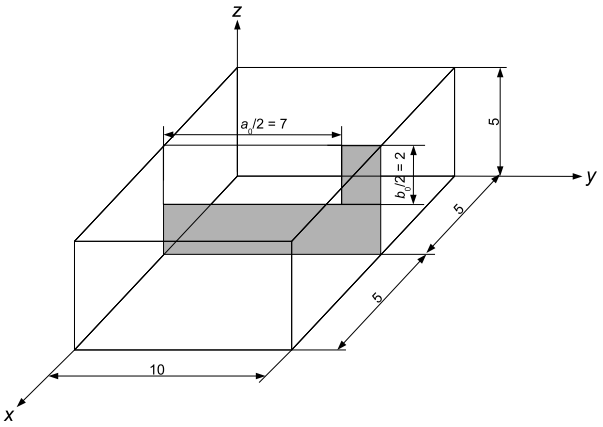

Figure 3. One quarter of the waveguide iris. Dimensions are in mm.

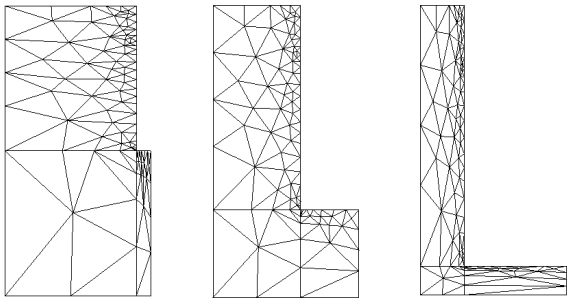

(a) $a = 10$, $b = 1$. (b) $a = 14$, $b = 4$. (c) $a = 18$, $b = 7$.

Figure 4. Surface mesh of one quarter of iris at different points in parameter space. Dimensions are in mm. Structures are rotated by 90 degrees.

the width a and the height b of the opening, as well as the operating frequency f in the range

$$a = 10 \ldots 18\,\mathrm{mm}, \tag{17a}$$
$$b = \ 1 \ldots \ 7\,\mathrm{mm}, \tag{17b}$$
$$f = \ 8 \ldots 17\,\mathrm{GHz}\,. \tag{17c}$$

Note that the variations in geometry are very large. Even though modes of higher order are propagable at some frequencies, structural symmetry prevents such waveforms from being excited. The expansion point is set at (a_0 = 14 mm, b_0 = 4 mm, f = 10 GHz), and FE discretization results in a total of 41454 second order degrees of freedom.

B. Mesh Deformation Error

In our present prototype implementation, the mesh is parameterized by displacing nodal positions with the help of simple, problem-specific functions, which are constructed in such a way that deformation decreases linearly in the direction from the iris to the outer boundary. Fig. 4(b) presents the nominal FE mesh at the expansion point, and Figs. 4(a) and 4(c) show extreme instantiations at two opposite points on the outer boundary of the parameter domain.

Our first test compares full FE solutions based on deformed meshes and adaptive remeshing, for approximately the same number of unknowns. Fig. 5(a) shows results for $|S_{11}|$, and Fig. 5(b) presents the error in S_{11} for the deformed mesh with respect to adaptive remeshing. The

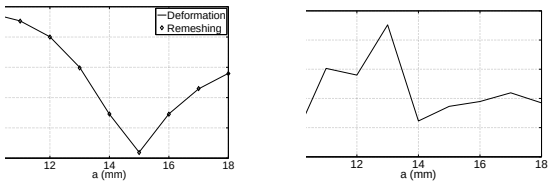

(a) $|S_{11}|$ (b) |Error in S_{11}|

Figure 5. Comparison of $|S_{11}|$ for full FE solutions based on deformed mesh and adaptive remeshing. Parameters: $b = 1\,\mathrm{mm}$ and $f = 10\,\mathrm{GHz}$.

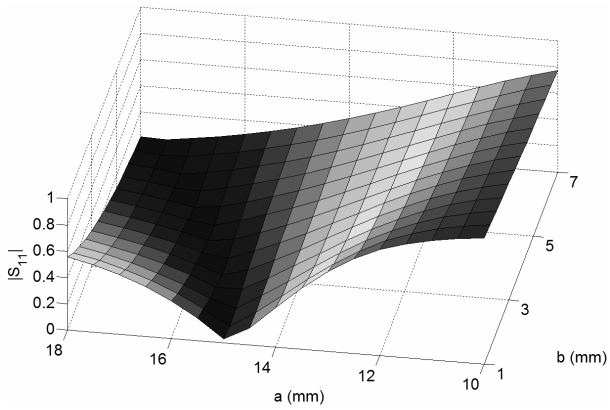

Figure 6. $|S_{11}|$ as function of width a and height b with deformed mesh at f = 10 GHz.

maximum error is in the order of $4 \cdot 10^{-3}$. It is mainly caused by poor mesh quality resulting from large deformations; see Figs. 4(a) and 4(c). A two-dimensional cut through the response hypersurface at $f = 10\,\mathrm{GHz}$ using deformed meshes is given in Fig. 6.

C. Interpolation Error

We next examine different interpolation schemes to achieve polynomial parameter dependence. For this purpose, we compare FE solutions based on the interpolated model (15) and instantiations of the parametric mesh, respectively.

Figs. 7, 8, and 9 present the locations of 5×7 equidistant interpolation points, of 6^{th} order serendipity points after [12], and of 5×7 Chebyshev points, i.e., the tensor product of the zeros of the Chebyshev polynomial of order $n + 1$, as well as the corresponding error surfaces for S_{11} at f = 10 GHz. Overall, errors are in the order of 10^{-3}. It can be seen that both equidistant and serendipity interpolation lead to very similar results. In case of the Chebyshev scheme, however, the error decreases by a factor of two and spreads out more evenly over the parameter domain.

D. Model Order Reduction Error

Our final test aims at quantifying the error committed at the MOR stage. For this purpose, we start from the polynomially parameterized model obtained from the Chebyshev interpolation points of Fig. 9 and compute two ROMs of order 6 and 8, respectively, for the three parameters a, b, and f. Fig. 10 shows the frequency response for (a = 17 mm, b = 6 mm), and Fig. 11 gives the corresponding errors. It can be seen that ROM errors are in the order of 10^{-5} and 10^{-7}, respectively, over the entire frequency

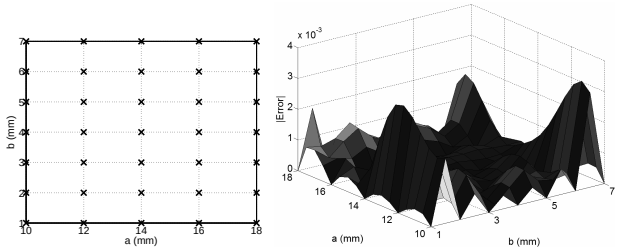

Figure 7. Interpolation by 5×7 equidistant and resulting interpolation error in S_{11} at f = 10 GHz.

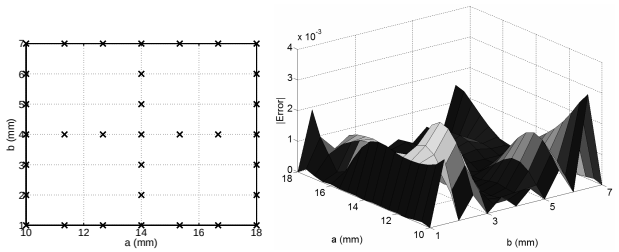

Figure 8. Interpolation by 6^{th} order serendipity points and resulting interpolation error in S_{11} at f = 10 GHz.

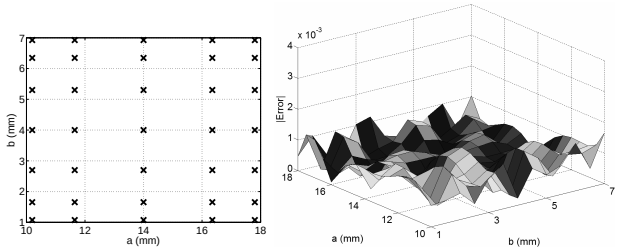

Figure 9. Interpolation by 5×7 Chebyshev points and resulting interpolation error in S_{11} at f = 10 GHz.

range, whereas the dominant error contributions stem from the matrix interpolation stage and are in the order of 10^{-3}.

E. Computational Data

Table I presents the CPU times for building the polynomially parameterized system and the subsequent MOR process, respectively. It can be seen that overall runtimes are dominated by the MOR step. For comparison, we have also included computational data for a full FE simulation. The immense speedup attainable by MOR is made clear by the runtimes and solution rates given in the last two rows of Table I. A single FE solution takes 42 s, whereas just 0.03 s are required to evaluate the 6^{th} order ROM. All computations were performed on an AMD Opteron 246 processor.

TABLE I: COMPUTATIONAL DATA FOR IRIS[1].

	ROM 6^{th} order	ROM 8^{th} order	Full FE
Dimension	168	330	78448
Interpolation[2] (s)	781.7	781.7	N.A.
Generation (s)	1973.8	3890.6	N.A.
Solution (s)	0.0277	0.125	42.47
Evaluations per s	36.1	7.99	0.0235

[1] MATLAB implementation on AMD Opteron 246 processor, 1.99GHz.

[2] 5×7 Chebyshev points.

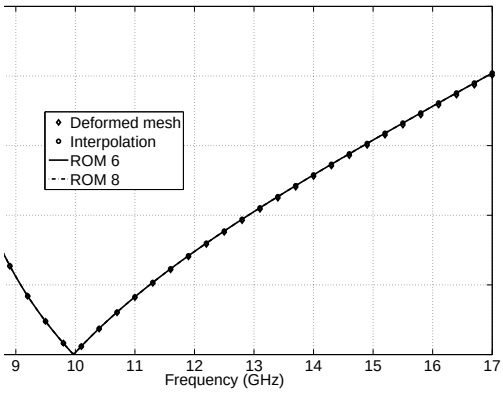

Figure 10. Magnitude of S_{11} versus frequency as a line in three-dimensional parameter space. Parameters: $a = 17\,\mathrm{mm}$, $b = 6\,\mathrm{mm}$.

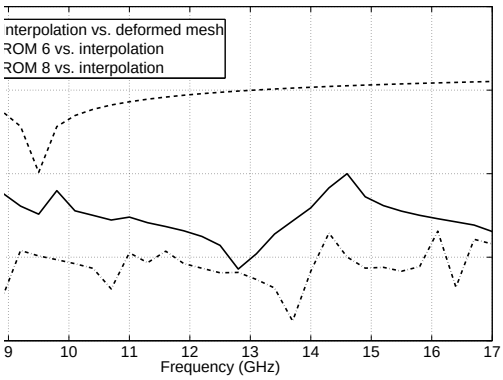

Figure 11. Error in S_{11} versus frequency as a line in three-dimensional parameter space. Parameters: $a = 17\,\mathrm{mm}$, $b = 6\,\mathrm{mm}$.

F. Bandpass Filter

Fig. 12 presents a bandpass filter consisting of three metal rods within an empty rectangular waveguide. We consider four model parameters: the diameters of the rods, d_1 and d_2, their distance l_{12}, and the operating frequency f. A rough hand calculation for a center frequency of 1.1 GHz and a passband return loss of 10 dB yields the expansion point(d_1 = 16 mm, d_2 = 40 mm, l_{12} = 180 mm, f = 1.1 GHz). To accommodate large variations in all model parameters, we define the parameter domain by

$$\begin{aligned} d_1 &= \ 9 \ldots 30\ \mathrm{mm}, \quad & l_{12} &= 150 \ldots 210\ \mathrm{mm}, \\ d_2 &= 23 \ldots 74\ \mathrm{mm}, \quad & f &= \ 0.8 \ldots 1.4\ \mathrm{GHz}. \end{aligned} \tag{18}$$

Even though the device could be analyzed more efficiently in the H plane, we employ a general three-dimensional FE model. Using the proposed MOR methodology, a single FE solution for the nominal design is sufficient to generate a whole family of 20 dB bandpass filters of greatly varying bandwidth BW and center frequency f_c. The ROM employs a tensor-product grid of $7 \times 7 \times 7$ Chebyshev points to interpolate the dependence of the FE matrices on the three geometrical parameters. Table II summarizes the parameter values and bandwidths of selected filter configurations with center frequencies from 1.0 to 1.34 GHz. Fig. 13 and Fig. 14 give the corresponding frequency responses and errors of a 5^{th} order ROM compared to full FE solutions at 201 equidistant frequency points. Even though the changes in filter geometry are very significant, errors in S_{11} are typically in the order of 10^{-4} to 10^{-3}. Table III gives com-

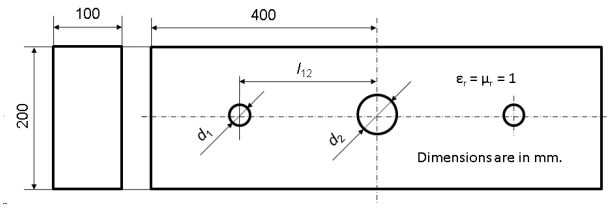

Figure 12: Structure of bandpass filter.

TABLE II: SELECTED FILTER CONFIGURATIONS*

f_c (GHz)	BW (MHz)	d_1 (mm)	d_2 (mm)	l_{21} (mm)
1.00	16.5	9.0	29.15	205.00
1.10	3.4	30.0	63.30	206.00
1.10	14.9	16.0	40.40	180.10
1.10	31.5	9.0	27.15	163.40
1.20	6.4	14.9	36.77	150.00
1.20	28.2	30.0	61.00	177.72
1.30	15.8	26.0	53.80	150.19
1.34	13.1	30.0	58.43	150.00

* Passband return loss: 20 dB max. Circular cross-sections are modelled by regular 16-gons of outer diameter d_i.

TABLE III: COMPUTATIONAL DATA FOR FILTER[1].

	ROM 4^{th} order	ROM 5^{th} order	Full FE
Dimension	140	252	44346
Interpolation[2] (s)	5388.5	5388.5	N.A.
Generation (s)	6241.0	8049.4	N.A.
Single solution (s)	3.491e-3	1.271e-2	4.1127
Freq. sweep[3] (s)	0.4536	1.402	8229.5

[1] MATLAB implementation on AMD Opteron 250 processor, 2.39 GHz.

[2] $7 \times 7 \times 7$ Chebyshev points.

[3] Frequency sweep of 2001 sampling points.

putational data and runtimes for the full FE system and ROMs of order 4 and 5, respectively. Even for the more expensive 5^{th} order ROM, the speedup for a single solution is 324! Even better, by diagonalizing the ROM matrices, we are able to compute a whole frequency sweep of 2001 sampling points in 1.4 s on an Opteron 250 processor, including the time for the eigenvalue decomposition. For comparison, 2001 FE solutions take 8229.5 s.

V. SUMMARY AND OUTLOOK

We have presented an interpolation technique that extends the scope of MOR methods for polynomial parameter dependence to geometry variations. The resulting ROMs are fast to evaluate and provide similar levels of accuracy as the original FE systems. Future applications will include shape optimization and inverse problems.

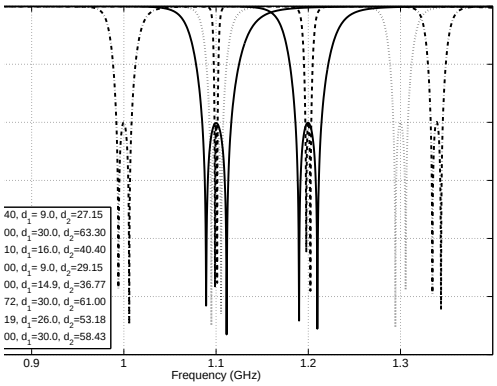

Figure 13. Magnitude of S_{11} versus frequency for selected filter configurations, based on a 5^{th} order ROM.

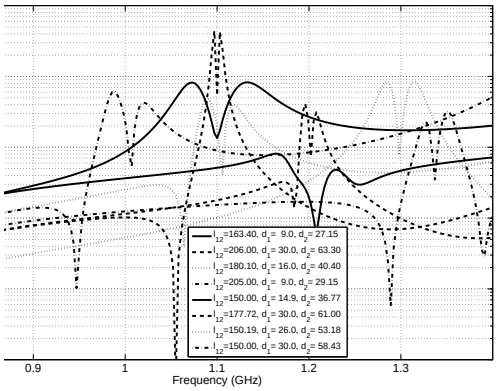

Figure 14. Error in S_{11} versus frequency for selected filter configurations, comparing a 5^{th} order ROM to full FE solutions.

REFERENCES

[1] P. Gunupudi, R. Khazaka, and M. Nakhla, "Analysis of transmission line circuits using multidimensional model reduction techniques," *IEEE Trans. Adv. Packaging,* vol. 25, no. 2, pp. 174-180, 2002.

[2] D.S. Weile, E. Michielssen, E. Grimme, and K. Gallivan, "A method for generating rational interpolant reduced order models of two-parameter linear systems", *Applied Mathematics Letters,* vol. 12, pp. 93-102, July 1999.

[3] D.S. Weile, E. Michielssen, "Analysis of frequency selective surfaces using two-parameter generalized rational Krylov model-order reduction", *IEEE Trans. Antennas Propagat.,* vol. 49, pp. 1539-1549, Nov. 2001.

[4] L. Daniel, C.S. Ong, L.S. Chay, K.H. Lee, J. White, "A Multiparameter Moment-Matching Model-Reduction Approach for Generating Geometrically Parameterized Interconnect Performance Models", *IEEE Trans. Comp.-Aided Design Integrated Circuits,* vol. 23, pp. 678-693, May 2004.

[5] L. Codecasa, "A novel approach for generating boundary condition independent compact dynamic thermal networks of packages, *IEEE Trans. Compononents Packaging*, vol. 28, pp. 593-604, Dec. 2005.

[6] Y.-T. Li, Z. Bai, Y. Su, Z. Zeng, "Model Order Reduction of Parameterized Interconnect Networks via a Two-Directional Arnoldi Process," IEEE Trans. Comp.-Aided Design Integrated Circuits, vol. 27, no. 9, pp. 1571-1582, Sep. 2008.

[7] O. Farle, V. Hill, P. Ingelström, R. Dyczij-Edlinger, "Multi-Parameter Polynomial Order Reduction of Linear Finite Element Models," *Mathematical and Computer Modelling of Dynamical Systems*, vol. 14, no. 5, pp. 421-434, Oct. 2008.

[8] M.A. González de Aza, J.A. Encinar, J. Zapata, and M. Lambae, "Full-wave analysis of cavity-backed and probe-fed microstrip patch arrays by a hybrid mode-matching generalized scattering matrix and finite-element method," *IEEE Trans. Antennas Propagat.,* vol. 46, pp. 234-242, 1998.

[9] A. H. Zaabab, Q. J. Zhang, and M. Nakhla, "A Neural Network Modeling Approach to Circuit Optimization and Statistical Design," *IEEE Trans. Microwave Theory Tech.*, vol. 43, no. 6, pp. 1349 - 1358, June 1995.

[10] D. Deschrijver, T. Dhaene, and D. De Zutter, "Robust Parametric Macromodeling Using Multivariate Orthonormal Vector Fitting," *IEEE Trans. Microwave Theory Tech.*, vol. 56, no. 7, pp. 1661 - 1667, July 2008.

[11] P.J. Davis, Interpolation and Approximation, New York: Dover Publ., 1975, pp. 24 - 94.

[12] W.J. Gordon and C.A. Hall, "Transfinite element methods: blending-function interpolation over arbitrary curved element domains," *Numer. Math.*, vol. 21, pp. 109-129, 1973.